Nonlinear Dynamic Analysis of Rolling Bearing–Rotor System

Huining An[1], Jianwei Lü[2*],Jiahui Zhang

[1]*Baotou Railway Vocational & Technical College, Baotou 730000, China*
[2]*Hohhot Vocational University of Technology, Hohhot 010070, China*
[*]*Corresponding author: ljwvvs@163.com*

Abstract: *This study focuses on an unbalanced rotor system supported by rolling bearings. The variable-step Runge–Kutta method is employed to perform numerical integration and obtain the system's dynamic responses. Bifurcation diagrams under different operating conditions are used to analyze the evolution of system behavior as parameters vary. The results indicate that at lower rotational speeds, the system exhibits quasi-periodic motion with small vibration amplitudes, posing minimal impact on operational stability. As the rotational speed increases, the motion becomes more complex, presenting various response forms such as periodic motion, quasi-periodic motion, and chaos, accompanied by larger vibration amplitudes and unstable system operation. These findings can serve as guidance for system operation under different rotational speeds and provide theoretical support for the stable performance of rolling bearing–rotor systems.*

Keywords: *rolling bearing; rotor system; bifurcation diagram; Poincaré map*

1. Introduction

In February 2025, China and Mongolia signed an agreement on the construction of a cross-border railway. Once operational, this railway will hold strategic significance for enhancing the connectivity capacity of the China–Mongolia–Russia Economic Corridor. The safety and operational stability of high-speed trains are directly linked to the efficiency of railway transportation, passenger safety, and the sustainability of international cooperation. As a core component of the power transmission system in high-speed trains, the rolling bearing–rotor system plays a decisive role in maintaining operational stability due to its nonlinear dynamic characteristics and vibration behavior. The study of its dynamic properties has attracted substantial attention, and significant progress has been made in recent years.

Chen Guo[1] developed a dynamic model of a rotor–rolling bearing system with coupled faults involving imbalance, rubbing, and base looseness, revealing the effects of rotational speed and bearing clearance on the system's bifurcation and chaotic behavior. Chen Zhe-ming[2] investigated the influence of traction motor rotor vibrations on vehicle dynamics. Liu Guo-yun[3] focused on the early fault detection of axle box bearings in high-speed trains. Luo Ren[4], based on the dynamics of multibody systems, established a coupled lateral–vertical–longitudinal dynamic model for trailers and motor cars. Zhao Huai-yun[5] analyzed the impact of harmonic torque in asynchronous traction motors on locomotive dynamics. Xu Hu[6] examined the causes behind the increasing failures of wheels and bearings in 25K-type passenger cars. Chen Guo[7] proposed an improved Empirical Wavelet Transform (EWT) method for the intelligent diagnosis of surface damage in rolling bearings. Zhang Ao[8] introduced methods for Doppler distortion correction, multisource sound separation, strong noise filtering, and feature extraction of wayside acoustic signals for train bearing faults.

These studies have established dynamic models of bearing–rotor systems with various degrees of freedom, focusing primarily on the system's bifurcation behavior and the transition from periodic motion to chaos. However, they fall short of comprehensively revealing the global dynamic behavior of the system. In particular, the coexistence of periodic solutions and their bifurcation evolution processes have been rarely addressed. Therefore, this paper adopts the nonlinear dynamic model of a rotor system with mass eccentricity proposed in[1] to analyze the motion states of the rolling bearing–rotor system under varying rotational speeds. Based on bifurcation diagrams, this study explores the coexistence bifurcation modes of periodic motion, and further examines the evolution patterns under different operating conditions using phase diagrams and Poincaré maps.

2. Dynamics of the Rolling Bearing–Rotor System

2.1 Rolling Bearing Model

2.1.1 Kinematic Analysis of the Rolling Bearing

The rolling bearing selected in this study is the JIS6306 bearing, with its parameters listed in Table 1.

Table 1 *Calculation Parameters of JIS6306 Rolling Bearing*

Outer ring radius Ro（mm）	Inner ring radius R_i（mm）	Ball radius r_b（mm）	Number of balls N_b	Bearing clearance γ（μm）
63.9	40.1	5.95	8	5

The linear velocity at the contact point between the rolling element and the outer raceway is v_o，The linear velocity at the contact point between the rolling element and the inner raceway is vi，Assumed angular velocity of the outer ring ω_o，Angular velocity of the inner ring ω_i，Outer ring radius R_o，Inner ring radius R_i，then:

$$\begin{cases} v_o = \omega_o R_o \\ v_i = \omega_i R_i \end{cases} \tag{1}$$

The linear velocity of the ball center in the retainer is:

$$v_c = \left(v_o + v_i\right)/2 \tag{2}$$

Since the outer ring of the bearing is fixed，Therefore $v_o=0$，Then:

$$v_c = v_i/2 = \left(\omega_i R_i\right)/2 \tag{3}$$

That is, the angular velocity of the cage is:

$$\omega_c = \frac{v_c}{\left(R_o + R_i\right)/2} = \frac{\left(\omega_i R_i\right)/2}{\left(R_o + R_i\right)/2} = \frac{\omega_i R_i}{R_o + R_i} \tag{4}$$

Since the inner ring of the bearing is fixed to the shaft,Therefore, the rotational speed of the inner ring is equal to that of the rotor,That is $\omega_i=\omega$，Then:

$$\omega_c = \frac{\omega R_i}{R_o + R_i} \tag{5}$$

During the rotation of a rolling bearing, the radial load acting on the rolling elements varies with their angular position, resulting in periodic vibrations, known as rolling element passage vibration, also referred to as VC vibration. Its frequency can be expressed as:

$$f_{vc} = \omega_c \times N_b \tag{6}$$

2.1.2 Load Analysis of Rolling Bearing

The simplified model of the rolling bearing is shown in Figure 1.

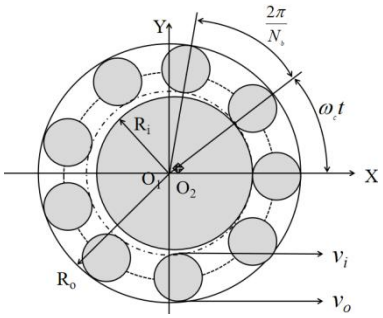

Figure 1 *Schematic Diagram of the Rolling Bearing Model*

Let the angular position of the *i*-th rolling element be θ_i， Then:

$$\theta_i = \omega_c t + \frac{2\pi}{N_b}(i-1) \tag{7}$$

The formula for the elastic deformation at the contact point is:

$$r_{\theta_i} = \frac{2\Gamma}{\pi}\left(\frac{3Q^2\sum\rho}{8}\left(\frac{1-\upsilon^2}{E}\right)^2\left(\frac{\pi k^2}{2\Sigma}\right)\right)^{1/3} \tag{8}$$

Where: Γ,Σ — Hertzian contact coefficients determined by the properties of the contact surfaces;E — Young's modulus, N/m²;υ— Poisson's ratio;$\Sigma\rho$— the sum of the curvature radii of the contact elements, m^{-1}.

According to Equation (8), the contact stiffness of the rolling bearing can be obtained as:

$$k_b = \frac{2E}{3\left(1-\upsilon^2\right)}\sqrt{\frac{2}{\left(\frac{2\Gamma k}{\Sigma\pi}\right)^3\Sigma\rho}} \tag{9}$$

In this paper, $E = 2.1\times10^{11}\,N/m^2$， $\upsilon = 0.3$， $\Sigma\rho = 266\,m^{-1}$， $2\Gamma k/\Sigma\pi = 1$.Substituting these parameters into Equation (9) yields the contact stiffness as:

$$k_b = 13.34\times10^9\,N/\mathrm{m}^{3/2} \tag{10}$$

As shown in the figure, the expression for the elastic deformation of the i-th rolling element in contact with the inner and outer raceways at any given moment is:

$$r_{\theta i} = x\cos\theta_i + y\sin\theta_i - \gamma \tag{11}$$

By summing the contact forces acting on each rolling element of the bearing, the total Hertzian contact forces of the left and right bearings in the x and y directions can be obtained as:

$$\begin{aligned}
f_{xR} &= -\sum_{i=1}^{N_b} k_{bR}[(x_R\cos\theta_i + y_R\sin\theta_i) - \gamma]_+^{.5}\cos\theta_i \\
f_{yR} &= -\sum_{i=1}^{N_b} k_{bR}[(x_R\cos\theta_i + y_R\sin\theta_i) - \gamma]_+^{.5}\sin\theta_i \\
f_{xL} &= -\sum_{i=1}^{N_b} k_{bL}[(x_L\cos\theta_i + y_L\sin\theta_i) - \gamma]_+^{.5}\cos\theta_i \\
f_{yL} &= -\sum_{i=1}^{N_b} k_{bL}[(x_L\cos\theta_2 + y_L\sin\theta_i) - \gamma]_+^{.5}\sin\theta_i
\end{aligned} \tag{12}$$

In the equation, N_b is the number of balls, and the subscript "+" indicates that the value inside the brackets is taken as a positive value. If the expression inside the brackets is greater than zero, the ball at angular position θ_i is under load and contributes an increment to the total contact force. If the expression inside the brackets is less than or equal to zero, the rolling element is not within the load zone, and the corresponding Hertzian contact force is zero.

2.2 Bearing–Rotor System Model

2.2.1 Dynamic Model and Equations of Motion

The rolling bearing–rotor system established in this study consists of two identical rolling bearings and a Jeffcott rotor. The simplified six-degree-of-freedom system is shown in Figure 2.

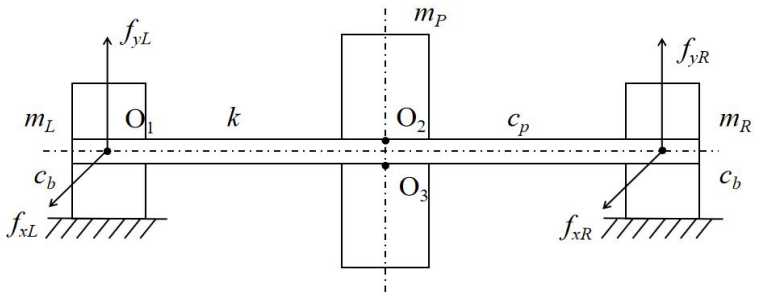

Figure 2 *Mechanical Simplified Model of the Rolling Bearing–Rotor System*

In Figure 2, O_1 and O_2 represent the geometric centers of the bearings and the rotor, respectively, and O_3 denotes the mass center of the rotor. m_p is the mass of the rotor; m_L and m_R are the rotor masses at the left and right bearings, respectively. c_b is the damping coefficient of the rotor at the bearings, and c_p is the damping coefficient of the rotor at the disk. k denotes the shaft stiffness. f_{xL} and f_{yL} are the total Hertzian contact forces of the left bearing in the x and y directions, respectively, and f_{xR} and f_{yR} are those of the right bearing.

According to Newton's second law, the nonlinear equations of motion of the system can be obtained as:

$$\begin{cases} m_R\ddot{x}_R + c_b\dot{x}_R + k\left(x_R - x_p\right) = f_{xR} \\ m_R\ddot{y}_R + c_b\dot{y}_R + k\left(y_R - y_p\right) = f_{yR} - m_R g \\ m_p\ddot{x}_p + c_p\dot{x}_p + k\left(x_p - x_R\right) + k\left(x_p - x_L\right) = m_p e\omega^2\cos\left(\omega t\right) \\ m_p\ddot{y}_p + c_p\dot{y}_p + k\left(y_p - y_R\right) + k\left(y_p - y_L\right) = m_p e\omega^2\sin\left(\omega t\right) - m_p g \\ m_L\ddot{x}_L + c_b\dot{x}_L + k\left(x_L - x_p\right) = f_{xL} \\ m_L\ddot{y}_L + c_b\dot{y}_L + k\left(y_L - y_p\right) = f_{yL} - m_L g \end{cases} \tag{13}$$

In the equations, x_p and y_p represent the displacements of the rotor at the disk in the x and y directions, respectively; x_R、y_R represent the displacements of the rotor at the right bearing in the x and y directions, respectively; x_L and y_L represent the displacements of the rotor at the left bearing in the x and y directions, respectively; e denotes the mass eccentricity of the system.

3. Solution and Analysis of the System's Nonlinear Dynamics

This section focuses on the dynamic behavior exhibited by the system as the rotational speed varies when the eccentricity e = 0.03 mm. The bifurcation diagram of the displacement x_p with respect to the rotational speed ω is shown in Figure 3.

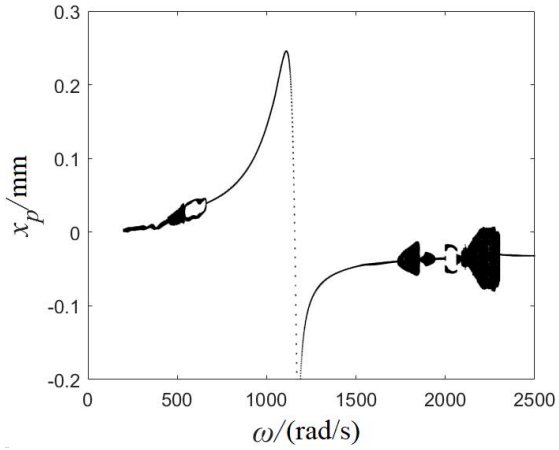

Figure 3 *Bifurcation Diagram of x_p with Respect to Rotational Speed*

In interval ω∈[2500,1938], as shown in Figure 3, the system exhibits period-one motion at high rotational speeds. As the rotational speed decreases, the motion transitions from period-one to quasi-periodic. Further reduction in the rotational speed ω leads to chaotic motion. During this phase, the system experiences highly unstable vibrations, which significantly affect operational stability and should be avoided. When the rotational speed decreases to 2060 rad/s, a reverse Hopf bifurcation occurs, resulting in period-two motion. At this point, the system's vibration amplitude decreases, the motion becomes more regular, and the operation stabilizes.

In interval ω∈[1938,1736], due to the vibration response caused by rotational imbalance and the VC vibration response induced by the periodic variation in overall bearing stiffness, the Poincaré map displays closed curves, indicating quasi-periodic motion. As the rotational speed ω further decreases to 1770 rad/s, the system enters a quasi-periodic state with period-seven behavior. Within this interval, the system shows large vibration amplitudes and irregular dynamic responses, leading to unstable operation.

Conclusion

Based on the above analysis, during the operation of the rolling bearing–rotor system, the excitation caused by rotational imbalance gradually intensifies with increasing rotational speed, and the system primarily vibrates under the influence of this unbalanced force. In particular, within speed interval ω∈[1938,1736], the system exhibits complex motion states, including periodic motion, quasi-periodic motion, and chaos, with relatively large vibration amplitudes. The system operates unstably in this range, exerting a significant impact on the bearing–rotor system. Therefore, appropriately adjusting the operating speed of the rotor system can maintain stable periodic motion, reduce adverse vibrations that may damage the rotor, and enhance the overall stability and reliability of the system.

Fund Project:

Influence of Vibration in Rolling Bearing–Rotor Systems on the Operational Stability of High-Speed Trains and Research on Fault Diagnosis, 2025 Scientific Research Project of Baotou Railway Vocational & Technical College, Project No.: BTZY202513.

References

[1] Chen Guo. Nonlinear dynamic response analysis of a rotor–rolling bearing system with coupled faults of imbalance, rubbing, and base looseness. Journal of Vibration and Shock, 2008, (09): 100–104+186.

[2] Chen Zhe-ming, Zeng Jing. Influence of traction motor rotor vibration on the dynamic performance of high-speed trains. Engineering Mechanics, 2011, 28(01): 238–244.

[3] Liu Guo-yun, Zeng Jing, Luo Ren, et al. Vibration characteristics analysis of high-speed vehicles with axle box bearing defects. Journal of Vibration and Shock, 2016, 35(09): 37–42+51.
[4] Luo Ren, Zeng Jing, Dai Huan-yun. Train system modeling and operational stability analysis. China Railway Science, 2006, (01): 72–77.
[5] Zhao Huai-yun, Liu Jian-xin, Zhai Wan-ming. Influence of harmonic torque in asynchronous traction motors on locomotive dynamics. Journal of Southwest Jiaotong University, 2009, 44(02): 269–273.
[6] Xu Hu. Analysis and countermeasures for increased failures of wheels and bearings in 25K-type passenger cars. Railway Vehicles, 2006, (01): 35–37+46.
[7] Chen Guo. A novel method for intelligent diagnosis of surface damage faults in rolling bearings. Chinese Journal of Scientific Instrument, 2009, 30(01): 44–49.
[8] Zhang Ao. Research on key technologies for wayside acoustic diagnosis of train bearing faults. University of Science and Technology of China, 2014.